Available online at www.sciencedirect.com

jmr&t Journal of Materials Research and Technology

journal homepage: www.elsevier.com/locate/jmrt

Original Article

Development of high thermal conductivity, enhanced strength and cost-effective die-cast Mg alloy compared with AE44 alloy

Lingyun Feng [a], *Xixi Dong* [a,*], *Mingxu Xia* [b], *Xiangzhen Zhu* [a], *Gang Ji* [c], *Hailin Yang* [d,**], *Bin Wang* [e], *Eric A. Nyberg* [f], *Shouxun Ji* [a,***]

[a] *Brunel Centre for Advanced Solidification Technology (BCAST), Brunel University London, Uxbridge, UB8 3PH, UK*
[b] *School of Materials Science and Engineering, Shanghai Jiao Tong University, Shanghai, 200240, China*
[c] *Univ. Lille, CNRS, INRAE, Centrale Lille, UMR 8207 - UMET - Unité Matériaux et Transformations, F-59000, Lille, France*
[d] *State Key Laboratory of Powder Metallurgy, Central South University, Changsha, 410083, China*
[e] *Department of Mechanical Engineering and Aerospace, Brunel University London, Uxbridge Middlesex UB8 3PH, UK*
[f] *Kaiser Aluminum, Spokane Valley, WA, 99216, USA*

ARTICLE INFO

Article history:
Received 28 November 2022
Accepted 20 December 2022
Available online 24 December 2022

Keywords:
Magnesium alloy
Die-cast
Conductivity
Microstructure
Mechanical properties

ABSTRACT

The thermal conductivity (TC) and strength trade-off has been a long-standing dilemma for developing high TC alloys. Here a novel high TC and cost-effective die-cast Mg2.8Al3.8-La0.4Nd alloy was developed with enhanced yield strength (YS) at room temperature (RT) and high temperatures (HT), compared with the commercially widely used die-cast AE44 magnesium alloy. The new alloy provided the TC of 104.0 and 125.9 W/(m·K) separately at RT and 300 °C. Compared with AE44 alloy, the TC was improved by ~13.5%. The new alloy also delivered an excellent YS of 137.1 MPa, ultimate tensile strength (UTS) of 240.2 MPa and elongation of 8.8% at RT, and the YS of the new ally was enhanced by 6.3% at RT and 9.8% at 300 °C, compared with AE44 alloy. The new alloy only has a 1.3% increase in raw material cost compared with AE44 alloy, offering a relatively cost-effective alternative. The lamellar $(Al,Mg)_3RE$ and $Al_{11}RE_3$, the needle-like $Al_{2.12}RE_{0.88}$ and the blocky $Al_{10}RE_2Mn_7$ intermetallic phases were identified. With the optimizing addition of Al and La, the Al solute amount in the matrix was reduced remarkably by 42% and then contributed to the improvement of TC. The major $(Al,Mg)_3RE$ phase at grain boundaries (GBs) contributed heavily to the enhancement of YS. This study elucidates the importance of the transfer of Al from the matrix to form higher content and novel Al-based intermetallic phases at GBs, for achieving die-cast Mg-Al-based alloys with excellent TC and strength.

* Corresponding author.
** Corresponding author.
*** Corresponding author.
E-mail addresses: xixi.dong@brunel.ac.uk (X. Dong), y-hailin@csu.edu.cn (H. Yang), shouxun.ji@brunel.ac.uk (S. Ji).

https://doi.org/10.1016/j.jmrt.2022.12.125

1. Introduction

The increasing development of alternative energy vehicles, 3C telecommunication products and relative fields has increased the quantity and layout density of electromagnetic devices with high-power densities, and the resulting high temperatures can lead to a decrease in the operational stability and reliability of the devices [1–3]. Therefore, improving device thermal conductivity (TC) in a lightweight context is an extremely urgent issue. Due to their low density, magnesium alloys could replace conventional thermally conducting alloys [1,4]. However, the widespread application of magnesium alloys needs to consider two key issues: application performance and cost. According to the current research on magnesium alloys, a reasonable optimization of the alloying in magnesium alloys is an effective way to balance performance and cost [5–7]. In addition, low unit-cost high-pressure die casting (HPDC) is ideal for quantity production [8,9]. Therefore, the die-cast thermally conductive magnesium alloy that combines performance and cost is the aim of this investigation.

In general, the solid solution, the crystal structure and defects and the intermetallic phase determine the TC of the alloy [10–12]. The subsequent heat treatment or deformation produces microstructural changes, such as changes in solid solution, grain size and Intermetallic size, which also affect the TC [13,14]. Dilute atoms can cause lattice distortion in the matrix due to solid solution, shortening the mean free path for electron and phonon transfer and thus decreasing TC [12]. Grain boundaries (GBs) or intermetallic phases on GBs can also impede thermal conduction [15]. Solution heat treatment can increase the number of solution atoms in the matrix, thereby decreasing TC [1,16]. In contrast, artificial ageing heat treatment reduces the solute amount, thereby reducing the precipitation of solute atoms and increasing TC [12]. In addition, deformations such as extrusion positively affect the TC of certain alloys [1,17]. Within these factors, the solid solution of solute atoms is usually considered to be the main factor contributing to the deterioration of TC [1,12].

Al is often used in alloys to improve the castability of magnesium alloys, so most currently applied commercial die-cast magnesium alloys are Mg-Al-based alloys [6,18]. However, Al has a high equilibrium solid solution in magnesium of 12.7 wt% at 437 °C [19]. Excessive addition of Al can increase Al solute in a matrix, thus affecting TC. The TC of the common die-cast AZ91D, AM60, MRI230D and AE44 alloys are still at a low level, 51, 61, 77 and 91.4 W/(m·K), respectively [20–22]. AE44 alloy has the highest TC. However, it cannot be compared to the widely used die-cast A380 alloy (96 W/(m·K)) [22]. Therefore, reasonable control of the Al content is a critical concern in developing high TC Mg-Al-based alloys. In previous studies, we have successfully developed a HPDC Mg3.2Al4.4La0.4Nd alloy with excellent mechanical and thermal properties [7]. However, it performed poorly on the cost compared to AE44 alloy. Therefore, it was concluded that there was a need to develop an alloy with improved TC and mechanical properties compared to AE44 alloy at the exact cost.

The methods and strategies used in this study will be consistent with our previous study [7]. In this work, we have developed a new highly TC and cost-effective die-cast Mg2.8Al3.8La0.4Nd alloy with an improved yield strength (YS) at room temperature (RT) and high temperature (HT) and compared it comprehensively with commercially representative die-cast AE44 alloy and previous developed high TC Mg3.2Al4.4La0.4Nd alloy. The design strategy, microstructure, thermal properties, tensile properties, and strengthening mechanisms of new alloys were investigated in depth.

2. Experimental

Pure ingots of Mg, Al and Zn and Mg-30 wt%La, Mg-25 wt%Nd and Mg-5wt.%Mn ingots were used to produce developed Mg2.8Al3.8La0.4Nd alloy and previously developed Mg3.2Al4.4La0.4Nd alloy [7]. The pure magnesium ingots were melted in electrical resistance furnaces fitted with steel liners, and then the other ingots were inserted into the pure magnesium melt. Subsequently, the melt was agitated three times to homogenise the composition and eliminate the impurities. The melt prepared was maintained at 720 °C for 30 min before pouring. The compositions of prepared melts were exhibited in Table 1, measured with Inductively Coupled Plasma-Optical Emission Spectrometry (ICP-OES). For comparison, AE44 alloy samples were die-cast using commercial ingots.

The HPDC experiment proceeded with a 4500 kN cold-chamber Frech machine [23]. Circulated oil preheated the die to 230 °C, and the compressed water preheated the shot sleeve to 180 °C. The casting pressure was 320 bar. Alloy melts were poured into the shot sleeve to prepare die-casting at 715 °C. One plate with a thickness of 4 mm for the TC test and eight round bars with a gauge size of Ø6.35 mm × 50 mm for the tensile test were cast under each shot [24].

The TC was determined by $\lambda = \rho^{*}\alpha^{*}C_p$, where ρ was the density, α was the thermal diffusivity (TD), and C_p was the specific heat capacity (SHC) [1,25]. The Archimedes method was applied to determine the RT density, while the thermal expansion was measured using a Shimadzu TMA-50 instrument to determine the HT density. The TD was tested on a Netzsch LFA-427 machine with the laser-flash method. The SHC was assessed with a differential scanning calorimeter (Netzsch 404C). Tension tests were conducted on Instron test machine. The tension tests were separately conducted at strain rates of 1 mm/min and 0.0002/s for RT and HT. The samples were held at a specific HT for 40 min before tensile tests. Three thermal and six tensile samples were tested to get mean thermal and tensile properties, respectively.

Table 1 – Composition (in wt.%) of die-cast Mg2.8Al3.8La0.4Nd alloy and the commercial AE44 alloy measured by ICP-OES.

Alloy	Al	La	Ce	Nd	Zn	Mn	Mg
Mg2.8Al3.8La0.4Nd	2.78	3.76	–	0.41	0.21	0.30	Bal.
AE44	3.70	1.11	2.19	0.40	0.11	0.31	Bal.

X-ray diffraction (XRD), scanning electron microscopy (SEM), and transmission electron microscope (TEM) were utilized to characterize the microstructure. The XRD analysis was performed in the 20°–100° 2 Theta range using a D8 diffractometer. Backscattered electron SEM (BSE-SEM) was performed on a Zeiss SUPRA machine outfitted with Energy-dispersive (EDS) after mechanical polishing. Ion polishing on a Gatan 691 was applied to prepare the TEM samples with a thickness of 50 μm. TEM was conducted on an FEI Tecnai G2. The ImageJ software was used to measure phase area fraction based on at least 10 SEM images and grain size distribution by using a linear intercept method.

3. Results

3.1. Alloy design by thermodynamic calculation

A quantitative design strategy of high TC die-cast Mg-Al-based alloys based on non-equilibrium Scheil model calculations has been presented in our recent work [7]. According to this strategy, high TC of die-cast Mg-Al-based alloys can be achieved by minimizing the Al solute amount in the matrix. Minimizing the Al solute amount can entirely inhibit the $Mg_{17}Al_{12}$ phase formation during solidification. In the current research, the alloy design followed this quantitative strategy. Fig. 1a shows the thermodynamic calculations for Mg3.7Al0.4Nd-x(La + Ce) alloy system. As described in our recent work, AE44 alloy also belongs to this system [7]. The thermodynamic calculations were carried out at 700 °C to RT and atmospheric pressure. It was calculated that a volume percentage of 0.857% of the $Mg_{17}Al_{12}$ phase could be formed in AE44 alloy with 3.3 wt% mixed metal of La and Ce. It indicates that AE44 alloy is not in the ideal state of high TC. To achieve high TC in Mg3.7Al0.4Nd-x(La + Ce) alloy system, at least 6.0 wt% misch metal needs to be added to minimize the Al solute amount and ultimately suppress the $Mg_{17}Al_{12}$ phase. However, this is inconsistent with the underlying aim of cost control. Therefore, based on the high TC alloy development strategy, alloying of Mg alloys needs to be further optimized to achieve a balance between performance and cost.

An appropriate reduction of Al and, thus, the addition of matching RE to achieve high TC and cost-effectiveness is considered an alternative method to designing die-cast Mg-Al-based alloys. Furthermore, La has proven to be the most efficient element for TC among the common RE elements (La, Ce, Nd, Pr, Gd, Y, Sm) due to its low equilibrium solubility in Mg [26]. Moreover, the price difference between pure La and Ce/La enriched mixed metals is insignificant in the current market. Therefore, the Mg2.8Al0.4Nd-yLa alloy system was proposed in the present work. Fig. 1b displays the thermodynamic calculations for the Mg2.8Al0.4Nd-yLa alloy system, in which at least 3.5 wt% La addition is required to suppress the Mg17Al12 phase completely and achieve an optimized high TC. Considering combustion losses of La, the nominal composition of the high TC and cost-effective die-cast Mg-Al-based alloy of the present invention was designed and patented as Mg2.8Al3.8La0.4Nd0.2Zn0.3Mn [27], which was expressed as Mg2.8Al3.8La0.4Nd in the rest of the text.

3.2. Thermal properties

Fig. 2 presents the thermal properties of die-cast Mg2.8Al3.8-La0.4Nd alloy from 20 °C to 300 °C and compares with the commercial die-cast AE44 alloy and previously developed Mg3.2Al4.4La0.4Nd alloy [7]. The TD, SHC and TC increased with increasing temperature while the density decreased almost linearly. The TD and TC of Mg2.8Al3.8La0.4Nd alloy were significantly higher than AE44 alloy and slightly lower than Mg3.2Al4.4La0.4Nd alloy. The SHC of Mg2.8Al3.8La0.4Nd alloy was slightly less than AE44 alloy below 150 °C, higher than AE44 alloy above 200 °C, but both were lower than Mg3.2Al4.4La0.4Nd alloy. The density of Mg2.8Al3.8La0.4Nd alloy was slightly higher than AE44 alloy and lower than Mg3.2Al4.4La0.4Nd alloy.

The TD of Mg2.8Al3.8La0.4Nd alloy increased from 60.8 to 65.9 mm^2/s and TC from 104.0 to 125.9 W/(m·K) as temperature increased from 20 °C to 300 °C. For comparative alloy AE44, the TD increased from 51.9 to 58.9 mm^2/s, and the TC increased from 91.4 to 111.2 W/(m·K) within an identical thermal range. At 20 °C, the TD and TC of Mg2.8Al3.8La0.4Nd alloy were 17.2% and 13.7% higher than AE44 alloy. At 300 °C, the TD and TC of Mg2.8Al3.8La0.4Nd alloy were 12.0% and

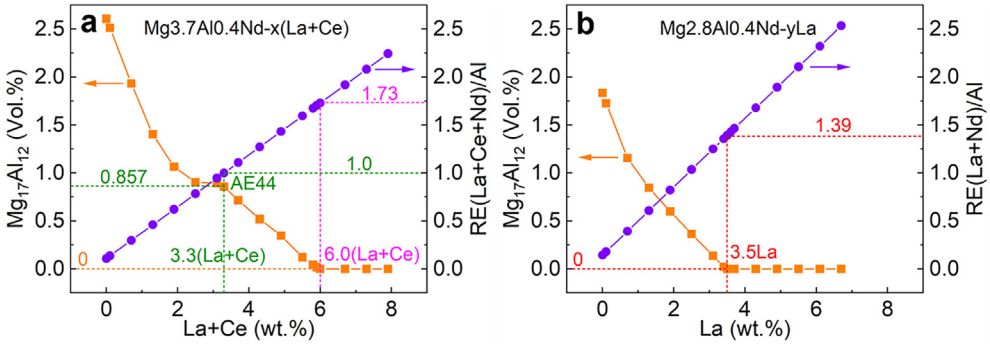

Fig. 1 – Thermodynamic calculation results of the volume percentage of the $Mg_{17}Al_{12}$ phase under non-equilibrium Schell mode. (a) Mg3.7Al0.4Nd-x(La + Ce) alloy [7], (b) Mg2.8Al0.4Nd-yLa alloy system that newly developed die-cast Mg2.8Al3.8La0.4Nd alloy belongs to.

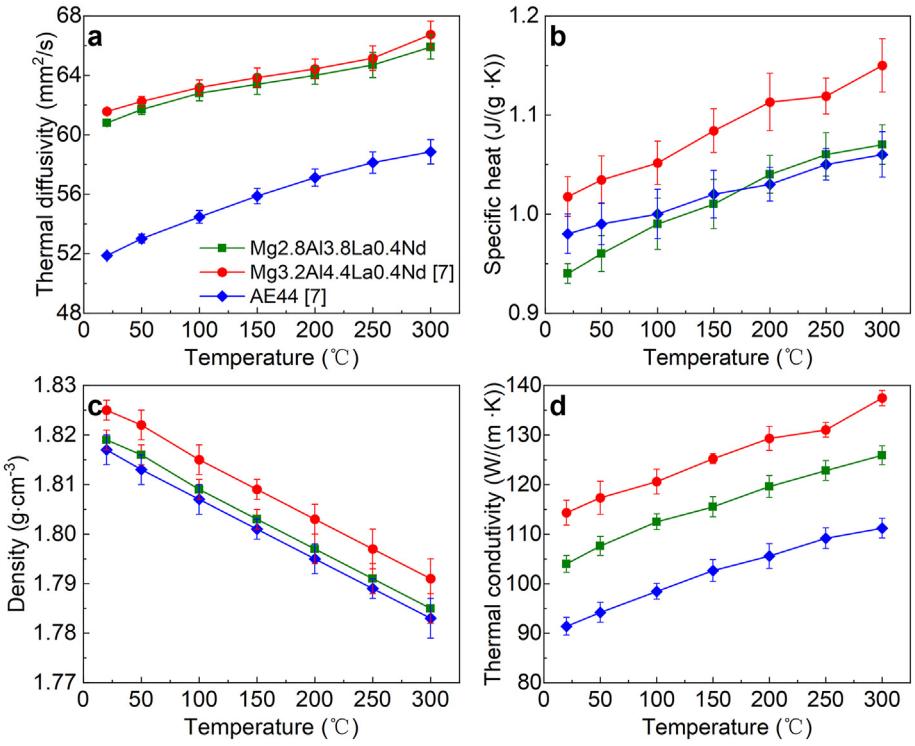

Fig. 2 – Thermal properties of die-cast Mg2.8Al3.8La0.4Nd alloy from 20 °C to 300 °C and in comparison with commercial die-cast AE44 alloy and previously researched Mg3.2Al4.4La0.4Nd alloy [7]. (a) TD, (b) SHC, (c) Density, and (d) TC.

13.2% higher than those of AE44 alloy. The improved TD was the main contributor to the improved TC. Table 2 and Supplementary Table S1 provided natural thermal properties data at RT and HT, respectively. It should be noted that the raw material cost of Mg2.8Al3.8La0.4Nd alloy is only 1.3% higher than comparator AE44 alloy and 1.4% lower than previously developed Mg3.2Al4.4La0.4Nd alloy, as shown in Supplementary Table S2.

3.3. *Enhancement of yield strength*

Fig. 3a–e displays the tensile curves of die-cast Mg2.8Al3.8La0.4Nd alloy at RT, 150 °C, 200 °C, 250 °C and 300 °C compared with commercial die-cast AE44 alloy and previously developed Mg3.2Al4.4La0.4Nd alloy [7]. Fig. 3f–h shows the YS, ultimate tensile strength (UTS) and elongation of the three alloys at varying temperatures. Detailed data on tensile properties are presented in Table 3. Mg2.8Al3.8La0.4Nd alloy can provide 137.1 MPa YS, 240.2 MPa UTS and 8.8% elongation at RT. Mg2.8Al3.8La0.4Nd alloy and previously developed Mg3.2Al4.4La0.4Nd alloys have higher YS and UTS at RT than comparator AE44 alloy, while lower elongation. Compared to AE44 alloy, Mg2.8Al3.8La0.4Nd alloy had a 6.3% enhancement in YS at RT. At 150–300 °C, Mg2.8Al3.8La0.4Nd alloy and previously developed Mg3.2Al4.4La0.4Nd alloy exhibited higher YS, UTS and elongation than comparative AE44 alloy. The YS, UTS and elongation of Mg2.8Al3.8La0.4Nd alloy at 300 °C were 72.5 MPa, 80.5 MPa and 37.1%, respectively, 9.8%, 8.5% and 144% greater than AE44 alloy. Therefore, Mg2.8Al3.8La0.4Nd alloy had a stronger YS at RT and a superior tensile property at HT than AE44 alloy. Incorporating the thermal and tensile properties from Tables 2 and 3, Fig. 3i shows that Mg2.8Al3.8La0.4Nd alloy provides enhanced YS and TC at RT compared to commercially available die-cast AE44 alloy and is cost-effective compared to previously developed Mg3.2Al4.4La0.4Nd alloy.

3.4. *Microstructure*

3.4.1. *XRD pattern*

Fig. 4 exhibits the XRD pattern of die-cast Mg2.8Al3.8La0.4Nd and AE44 alloys under as-cast conditions. α-Mg, $Al_{11}RE_3$ and Al_2RE phases were detected in AE44 alloy, which agreed with the reported phase constitution of AE44 alloy [28,29]. $Al_{11}RE_3$ phase was also detected in Mg2.8Al3.8La0.4Nd alloy. However, different from AE44 alloy, a significant presence of $(Al,Mg)_3La$ phase was detected, while the Al_2RE phase was hardly detected in Mg2.8Al3.8La0.4Nd alloy. It should be noted that small size or volume fraction phases are typically difficult to detect using XRD.

3.4.2. *SEM morphology*

Fig. 5a and b displays BSE-SEM micrographs of commercial AE44 alloy under the as-cast state. The AE44 matrix exhibited a typical die-cast Mg alloy microstructure comprising α_1-Mg nucleated inside sleeve and α_2-Mg nucleated inside chamber [5,23]. With a relatively high cooling rate, the dimension of α_2-Mg was smaller than α_1-Mg in the cavity [23,30]. In consistence with the previous reports [28,29], three intermetallic phases were found in AE44 alloy, i.e., the lamellar $Al_{11}RE_3$, the blocky Al_2RE and $Al_{10}RE_2Mn_7$ phases, and $Al_{11}RE_3$ was the major

Table 2 – Thermal properties at RT and raw material cost of die-cast Mg2.8Al3.8La0.4Nd and in comparison with die-cast AE44 alloy and previously researched Mg3.2Al4.4La0.4Nd alloy.

Alloys	Thermal diffusivity α/mm^2·s^{-1}	Special heat capacity C_p/J (g·K)$^{-1}$	Density ρ/g·cm^{-3}	Thermal Conductivity λ/W (m·K)$^{-1}$	Raw material cost	Ref
Mg2.8Al3.8La0.4Nd	60.8 ± 0.2	0.94 ± 0.01	1.819 ± 0.002	104.0 ± 1.7	101.3%	This work
Mg3.2Al4.4La0.4Nd	61.6 ± 0.2	1.02 ± 0.01	1.825 ± 0.002	114.3 ± 2.5	102.7%	[7]
AE44	51.9 ± 0.1	0.97 ± 0.01	1.817 ± 0.003	91.4 ± 1.8	100.0%	[7]

intermetallic phase, while Al_2RE and $Al_{10}RE_2Mn_7$ were the minor intermetallic phases, as shown in Fig. 5b.

Fig. 5c and d presents BSE-SEM morphology of die-cast Mg2.8Al3.8La0.4Nd alloy under the as-cast state. Different from AE44 alloy, in Mg2.8Al3.8La0.4Nd alloy, the lamellar $(Al,Mg)_3RE$ phase substituted for $Al_{11}RE_3$, a major intermetallic phase, while $Al_{11}RE_3$ was relegated to a minor one. In addition, a small amount of the needle-like $Al_{2.12}RE_{0.88}$ phase and the blocky $Al_{10}RE_2Mn_7$ phase were observed in Mg2.8Al3.8La0.4Nd alloy, and XRD did not detect these two intermetallic phases due to their small quantity. The four intermetallic phases in Mg2.8Al3.8La0.4Nd alloy were determined by TEM in the following text.

3.4.3. *TEM confirmation of $(Al,Mg)_3RE$ and $Al_{11}RE_3$*

Fig. 6a presents the scanning TEM (STEM) micrograph of $(Al,Mg)_3RE$ and $Al_{11}RE_3$ intermetallic phases in die-cast Mg2.8Al3.8La0.4Nd alloy under as-cast state, and Fig. 6b shows the mapping results of STEM-EDS of distribution elements in Fig. 6a. $Al_{11}RE_3$ and $(Al,Mg)_3RE$ phases were enriched in Al, La, Nd, Mn and minor Zn, while the contrast difference between $Al_{11}RE_3$ and $(Al,Mg)_3RE$ on Mg indicated the Mg presence in the $(Al,Mg)_3RE$ phase. Fig. 6c displays the bright-field TEM micrograph of $(Al,Mg)_3RE$ phase in Mg2.8Al3.8La0.4Nd alloy, and the corresponding indexed selected-area electron diffraction (SAED) pattern in Fig. 6d confirmed the lamellar

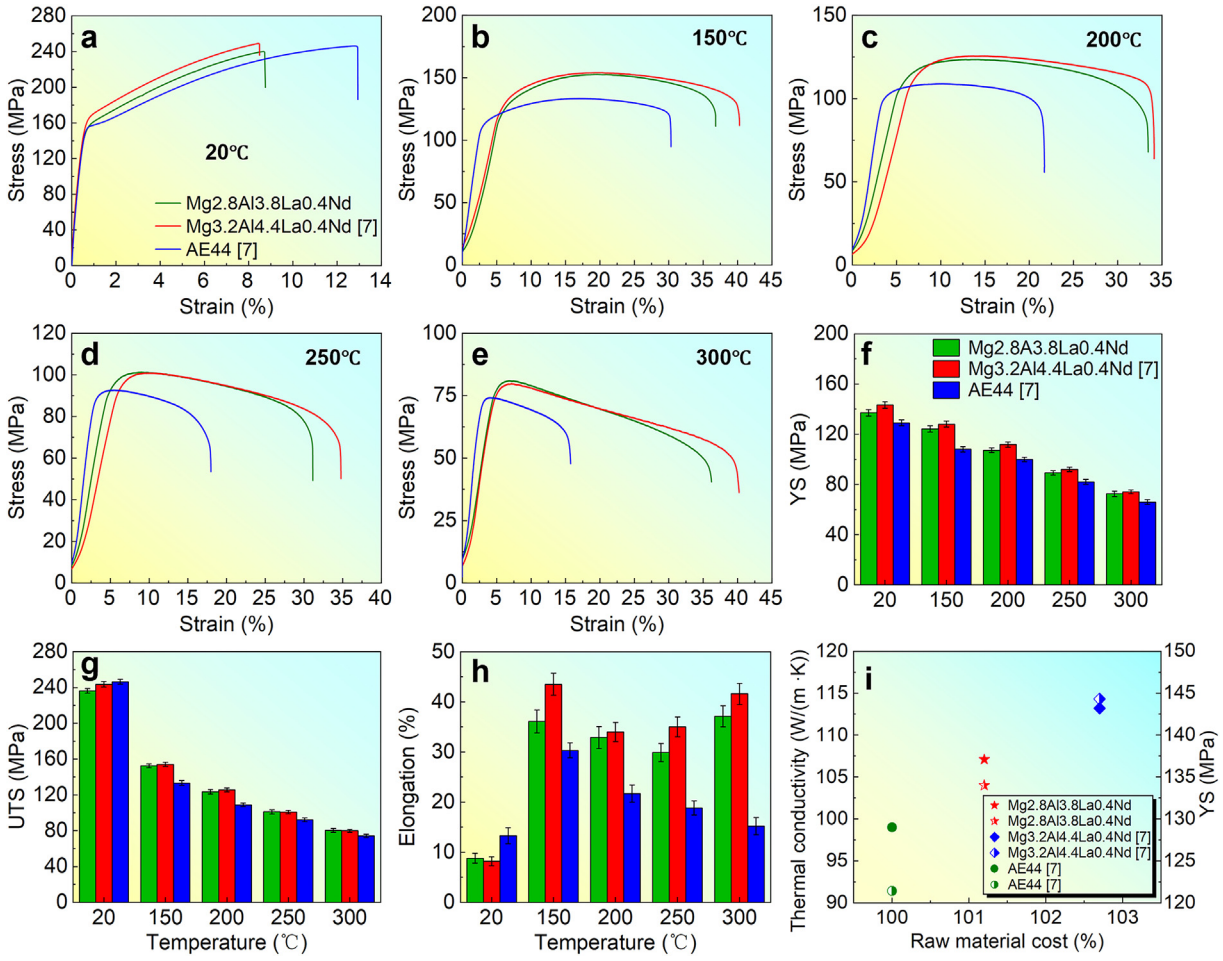

Fig. 3 – Tensile properties of Mg2.8Al3.8La0.4Nd alloy at RT and HT and in comparison with commercial AE44 alloy and previously researched Mg3.2Al4.4La0.4Nd alloy [7]. Representative tensile curves at (a) RT, (b) 150 °C, (c) 200 °C, (d) 250 °C and (e) 300 °C; (f) YS; (g) UTS; (h) elongation; (i) enhancement of YS and TC of cost-effective Mg2.8Al3.8La0.4Nd alloy at RT compare with commercial AE44 alloy and previously researched Mg3.2Al4.4La0.4Nd alloy.

Table 3 – YS, UTS and elongation of Mg2.8Al3.8La0.4Nd alloy at RT and HT, compared with commercial AE44 alloy and previously researched Mg3.2Al4.4La0.4Nd alloy.

Alloy	Tensile properties	20 °C	150 °C	200 °C	250 °C	300 °C
Mg2.8Al3.8La0.4Nd	YS (MPa)	137.1 ± 2.6	124.2 ± 2.4	107.2 ± 1.9	89.2 ± 1.7	72.5 ± 2.1
	UTS (MPa)	240.2 ± 2.5	152.6 ± 2.1	123.4 ± 2.5	101.1 ± 2.3	80.5 ± 2.0
	Elongation (%)	8.8 ± 1.0	36.1 ± 2.3	32.9 ± 2.2	29.9 ± 1.8	37.1 ± 2.1
Mg3.2Al4.4La0.4Nd [7]	YS (MPa)	143.2 ± 2.6	128.0 ± 2.3	111.7 ± 2.0	92.0 ± 1.8	74.1 ± 1.5
	UTS (MPa)	243.6 ± 3.0	157.1 ± 2.4	125.7 ± 2.1	100.9 ± 1.9	79.9 ± 1.5
	Elongation (%)	8.2 ± 0.9	43.5 ± 2.2	34.0 ± 1.9	35.0 ± 2.0	41.6 ± 2.1
AE44 [7]	YS (MPa)	129.0 ± 2.4	108.0 ± 2.2	99.9 ± 1.8	82.1 ± 2.0	66.0 ± 1.6
	UTS (MPa)	246.5 ± 2.5	133.3 ± 2.7	108.9 ± 1.9	92.4 ± 2.1	74.2 ± 1.7
	Elongation (%)	13.3 ± 1.6	30.3 ± 1.5	21.7 ± 1.7	18.8 ± 1.4	15.2 ± 1.7

phase was $(Al,Mg)_3RE$ phase (Orthorhombic, $a = 0.4336$ nm, $b = 1.8867$ nm, $c = 0.4424$ nm, $C222_1$) [31]. High-resolution TEM (HRTEM) micrograph in Fig. 6e and the corresponding fast Fourier transform (FFT) pattern in Fig. 6h confirmed the $(Al,Mg)_3RE$ phase. As reported, the $(Al,Mg)_3La$ formation might be relevant with the singular addition of La and/or the ratio of La and Al [31,32]. The bright-field TEM image in Fig. 6f and the SAED pattern in Fig. 6g verified the presence of the $Al_{11}RE_3$ phase (Orthorhombic, $a = 0.4431$ nm, $b = 1.3142$ nm, $c = 1.0132$ nm, *Immm*) in Mg2.8Al3.8La0.4Nd alloy [32,33]. Different from SEM, the Mg matrix under TEM is marked as Mg rather than α_1-Mg or α_2-Mg, as it is hard to identify α_1-Mg or α_2-Mg under the high magnification of TEM observation.

3.4.4. *TEM confirmation of $Al_{2.12}RE_{0.88}$*

Fig. 7a shows the STEM image of the needle-like $Al_{2.12}RE_{0.88}$ intermetallic phase in die-cast Mg2.8Al3.8La0.4Nd alloy under the as-cast condition, and Fig. 7b presents the mapping results of STEM-EDS of elements in Fig. 7a. The $Al_{2.12}RE_{0.88}$ phase was enriched in Al, La, Nd, Mn and minor Zn, and Mg was hardly present in the $Al_{2.12}RE_{0.88}$ phase. The SAED pattern in Fig. 7c verified that the needle-like phase in die-cast Mg2.8Al3.8-La0.4Nd alloy was $Al_{2.12}RE_{0.88}$ (Hexagonal, $a = b = 0.4382$ nm, $c = 0.4349$ nm, *P6/mmm*) [31]. The HRTEM image in Fig. 7d confirmed the $Al_{2.12}RE_{0.88}$ phase in Mg2.8Al3.8La0.4Nd alloy.

3.4.5. *TEM confirmation of $Al_{10}RE_2Mn_7$*

Fig. 8a presents the STEM image of the blocky $Al_{10}RE_2Mn_7$ intermetallic phase in die-cast Mg2.8Al3.8La0.4Nd alloy under an as-cast state. Fig. 8b shows the mapping results of STEM-EDS for the elemental distribution in Fig. 8a. The $Al_{10}RE_2Mn_7$ phase was enriched in Al, La, Nd, Mn and minor Zn. The SAED pattern in Fig. 8c verified that the blocky phase in die-cast Mg2.8Al3.8La0.4Nd alloy was $Al_{10}RE_2Mn_7$ (Hexagonal, $a = b = 0.9049$ nm, $c = 1.321$ nm, *R-3m*) [34,35]. The STEM-EDS result in Fig. 8d agreed well with the composition of $Al_{10}RE_2Mn_7$, which further supported the presence of the $Al_{10}RE_2Mn_7$ phase in Mg2.8Al3.8La0.4Nd alloy.

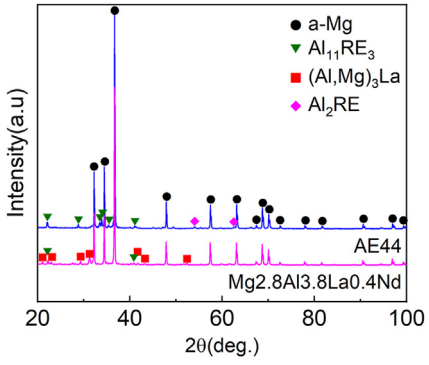

Fig. 4 – XRD results of die-cast Mg2.8Al3.8La0.4Nd alloy under as-cast conditions compared with commercial die-cast AE44 alloy.

3.4.6. *Fracture morphology*

Fig. 9a–d shows the SEM images of the fracture surface of die-cast Mg2.8Al3.8La0.4Nd alloy at RT, 150 °C, 250 °C and 300 °C, sequentially. In the RT tensile fracture, dimples can be easily found, while the cleavage planes were also observed, which indicated the coupling of the ductile and cleavage fracture mechanisms, and this was consistent with the moderate elongation of 8.8% at RT. The tensile fracture at 150 °C, 250 °C and 300 °C mainly comprised the dimples, and this demonstrated the ductile fracture mechanism at the HT of 150–300 °C. The tear ridge was observed in the tensile fracture at 150–300 °C. Moreover, the tear ridge at 150 °C and 300 °C was more evident than at 250 °C, which agreed with higher elongation at 150 °C and 300 °C than 250 °C.

4. Discussion

4.1. *Mechanisms of thermal conductivity improvement*

4.1.1. *Effects of solid solution in Mg matrix*

Solute amounts in the matrix were treated as a major factor in TC reduction [1]. The dissolved solute atoms can cause lattice distortion and reduce the mean free path of electrons and phonons [36], thus affecting heat transfer [12]. Al was the dominant solute in die-cast Mg-Al-based alloy owing to its high equilibrium solid solution of 12.7 wt% in Mg at 437 °C [19]. The SEM/TEM-EDS measured Al solute amount in matrix of AE44 alloy was 0.69 wt%, while the Al solute amount in matrix of Mg2.8Al3.8La0.4Nd is 0.40 wt%, a 42% reduction. The overall RE(La,Ce,Nd), Mn, and Zn solute amounts in matrix of Mg2.8Al3.8La0.4Nd and AE44 alloys were similar, as shown in Fig. 10. In contrast, previously developed Mg3.2Al4.4La0.4Nd alloy had a relatively lower content of Al solute in matrix, while total RE, Mn and Zn solute amounts were comparable to that of Mg2.8Al3.8La0.4Nd alloy [7]. Therefore, minimizing the Al

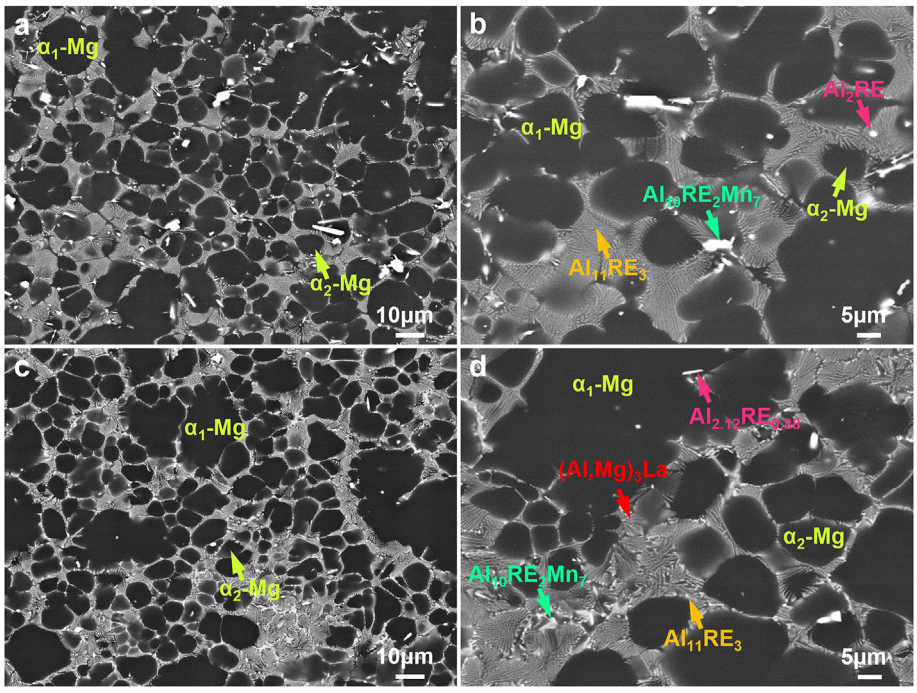

Fig. 5 – BSE-SEM micrographs of die-cast Mg2.8Al3.8La0.4Nd and AE44 alloys under as-cast state. (a,b) AE44; (c,d) Mg2.8Al3.8La0.4Nd.

solute amount in the matrix by completely suppressing the $Mg_{17}Al_{12}$ phase contributed significantly to improving TD and TC. It also validated the alloy design strategy mentioned in Section 3.1. It can be concluded that the newly developed Mg2.8Al3.8La0.4Nd alloy matrix had a lower content of Al solid solution compared to the AE44 alloy based on the high TC magnesium alloy development strategy and the optimization of the Al and corresponding RE additions, resulting in better TC.

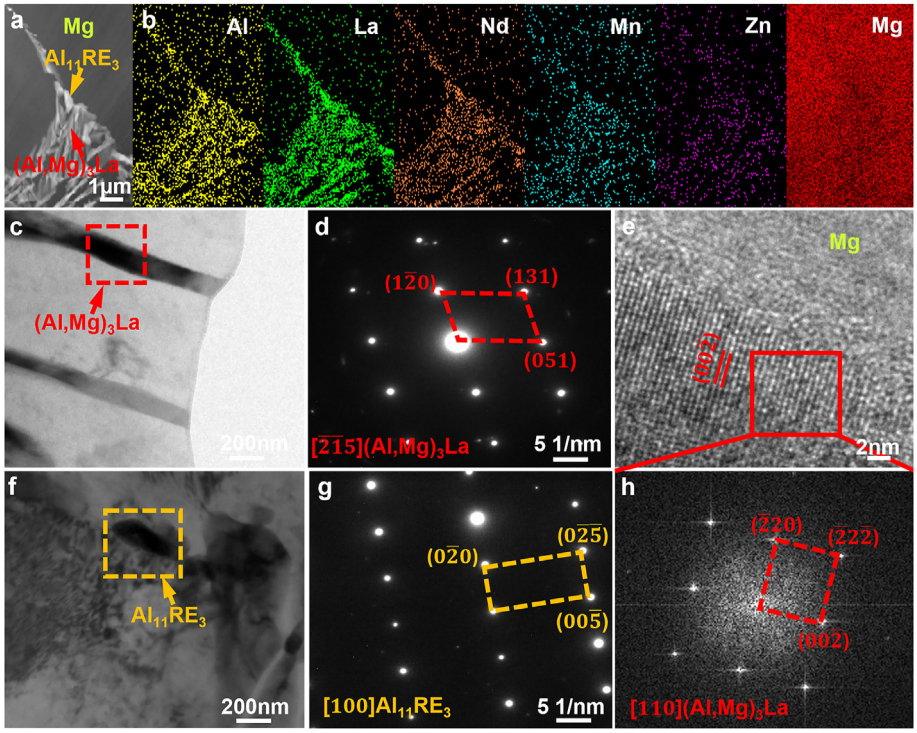

Fig. 6 – TEM confirmation of $(Al,Mg)_3La$ and $Al_{11}RE_3$ intermetallic phases in die-cast Mg2.8Al3.8La0.4Nd alloy in as-cast condition. (a) STEM micrograph; (b) STEM-EDS scanning of (a); (c) Bright-field TEM micrograph, (d) SAED, (e) HRTEM micrograph and (h) FFT pattern of $(Al,Mg)_3La$ phase; (f) Bright-field TEM micrograph and (g) SAED of $Al_{11}RE_3$ phase.

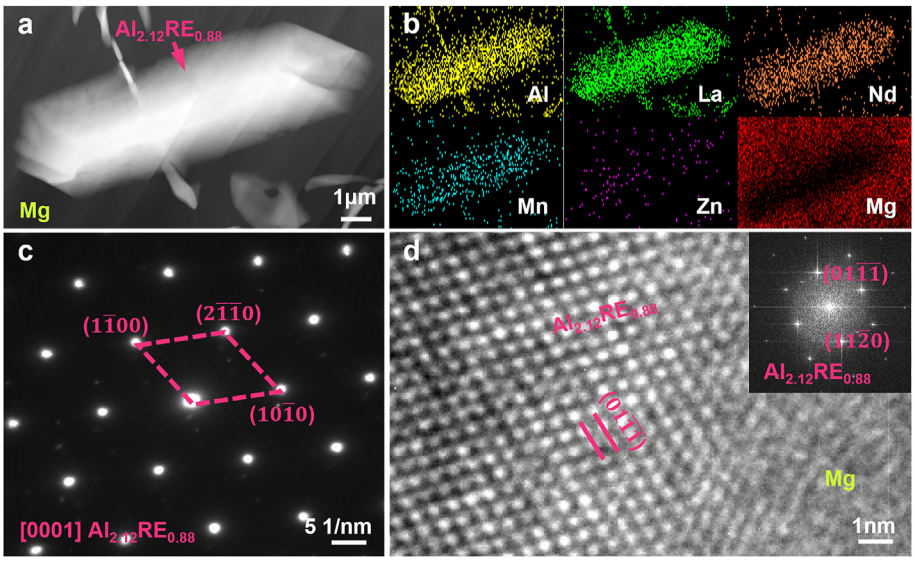

Fig. 7 – TEM confirmation of $Al_{2.12}RE_{0.88}$ intermetallic phase in die-cast Mg2.8Al3.8La0.4Nd alloy at the as-cast condition. (a) STEM image of $Al_{2.12}RE_{0.88}$ phase; (b) STEM-EDS mapping of (a); (c) SAED of $Al_{2.12}RE_{0.88}$ phase observed along [0001] zone axis; (d) HRTEM image of $Al_{2.12}RE_{0.88}$ phase with the corresponding FFT pattern as the insert.

4.1.2. *Effects of intermetallic phases at GBs*

The GBs and intermetallic phases at GBs also affect heat transfer [15,37]. Fig. 11a and b exhibit grain size distribution of die-cast AE44 and Mg2.8Al3.8La0.4Nd alloys, respectively. Fig. 11c displays the statistical average grain size (AGS) and area fraction of intermetallic phases in AE44 and Mg2.8Al3.8La0.4Nd alloys. The AGS of Mg2.8Al3.8La0.4Nd alloy was slightly higher than AE44 alloy, which should contribute faintly to improving

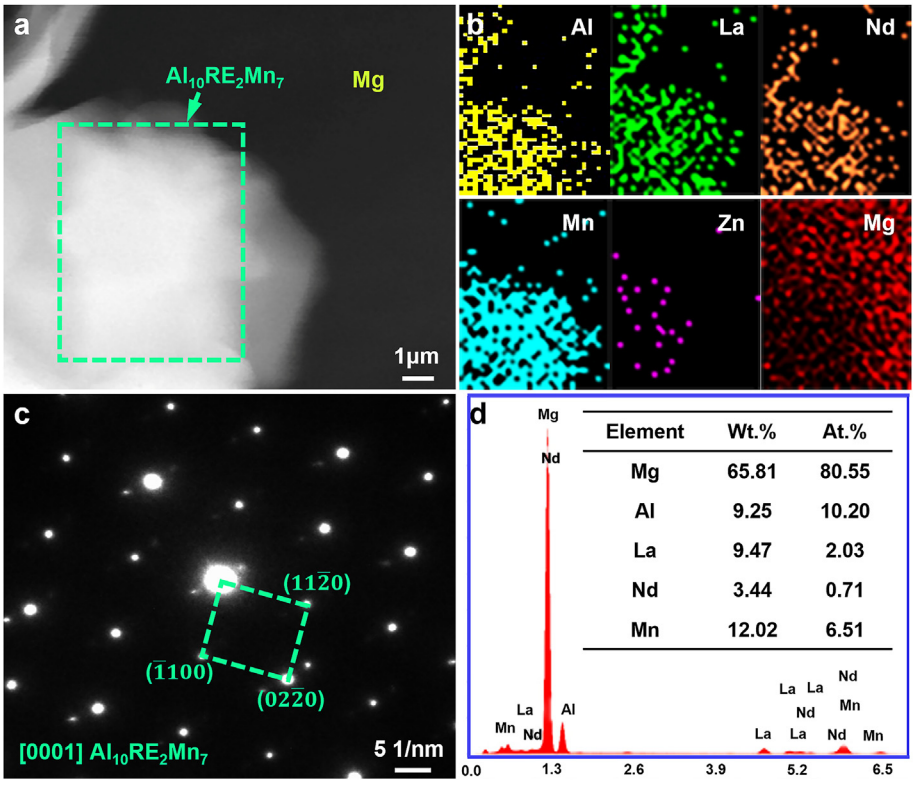

Fig. 8 – TEM confirmation of $Al_{10}RE_2Mn_7$ phase in die-cast Mg2.8Al3.8La0.4Nd alloy at as-cast condition. (a) STEM micrograph of $Al_{10}RE_2Mn_7$ phase; (b) STEM-EDS mapping of (a); (c) SAED of the $Al_{10}RE_2Mn_7$ phase observed along [0001] zone axis; (d) STEM-EDS result of the $Al_{10}RE_2Mn_7$ phase.

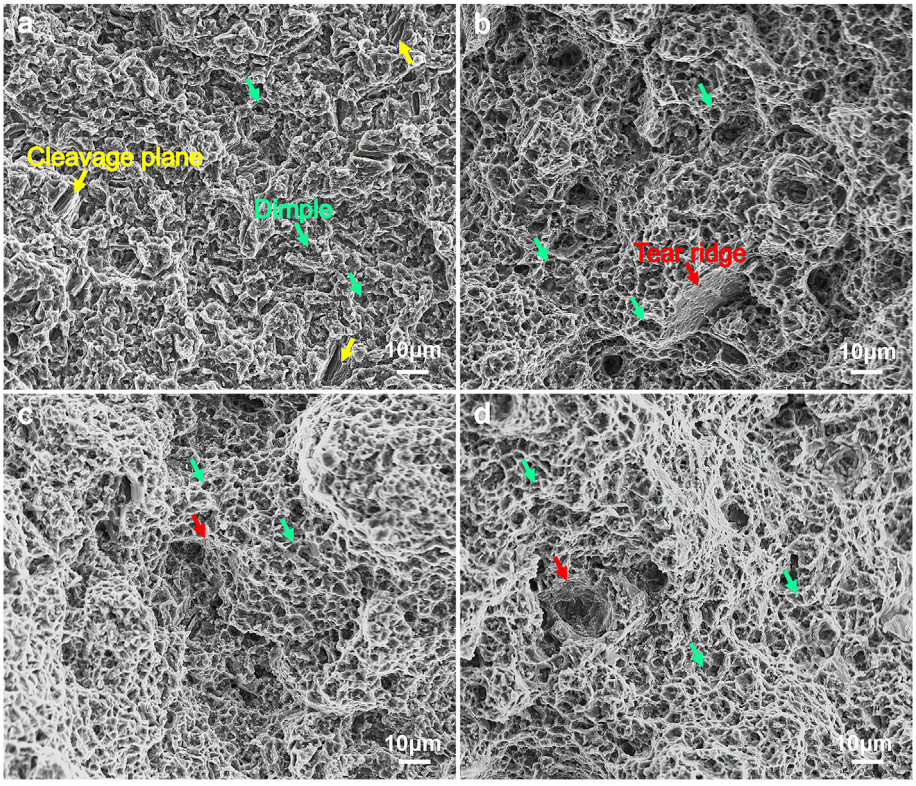

Fig. 9 – SEM images presenting the tensile fracture of die-cast Mg2.8Al3.8La0.4Nd alloy at RT and HT. (a) RT; (b) 150 °C; (c) 250 °C; (d) 300 °C.

the TC in Mg2.8Al3.8La0.4Nd alloy due to the decrease of the heat transfer block at GBs. The average area fraction of intermetallic phases in Mg2.8Al3.8La0.4Nd alloy was also slightly higher than in AE44 alloy. It should be mentioned that different from AE44 alloy, $(Al,Mg)_3RE$ replaced $Al_{11}RE_3$ as the major intermetallic phase in Mg2.8Al3.8La0.4Nd alloy. However, $(Al,Mg)_3RE$ had the same orthorhombic crystal structure as the $Al_{11}RE_3$ phase [32]. In addition, the substitution formation of major $(Al,Mg)_3RE$ phases in the Mg2.8Al3.8La0.4Nd alloy has not reduced the misfit or strengthened the thermal transmission from the intermetallic phase at the GBs to Mg matrix based on the misfit analysis of $(Al,Mg)_3RE/Al_{11}RE_3$ and Mg [7]. Therefore, the grain size and the major $(Al,Mg)_3RE$ intermetallic phase formed at GBs should have a limited impact on TC improvement compared with AE44 alloy. The improvement of TC in the Mg2.8Al3.8La0.4Nd alloy can be explained by minimizing Al solute amount in the matrix via optimizing Al and RE addition.

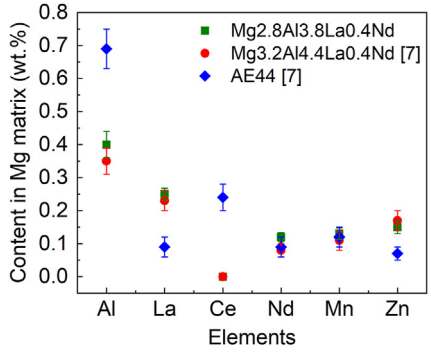

Fig. 10 – Solute amounts of the various elements in matrix of die-cast Mg2.8Al3.8La0.4Nd alloy under as-cast conditions and compared with commercial die-cast AE44 alloy and previously researched Mg3.2Al4.4La0.4Nd alloy.

4.2. *Mechanisms of enhancement of yield strength*

According to Section 3.3, the YS of Mg2.8Al3.8La0.4Nd alloy at RT and 300 °C was enhanced by 6.3% and 9.8%, respectively, compared with AE44 alloy. It is well known that the strengthening of alloys is generally determined by solid solution strengthening(σ_{ss}), grain refinement strengthening (σ_{gr}), second phase strengthening (σ_{sp}) at GBs, precipitation strengthening and deformation strengthening [38–40]. Precipitation and deformation strengthening can be neglected at room temperature. Thus, the strengthening YS can be expressed by the following equation:

$$\Delta\sigma_{Mg2.8Al3.8La0.4Nd} = \Delta\sigma_{ss} + \Delta\sigma_{gr} + \Delta\sigma_{sp} \quad (1)$$

The multi-solid-solution model presented by Gypen and Deruyttere [41]can be used to express $\Delta\sigma_{ss}$ effect on die-cast Mg alloys:

$$\Delta\sigma_{SS} = \left(\sum_i \left(k_i^{1/n} C_i\right)\right)^n \quad (2)$$

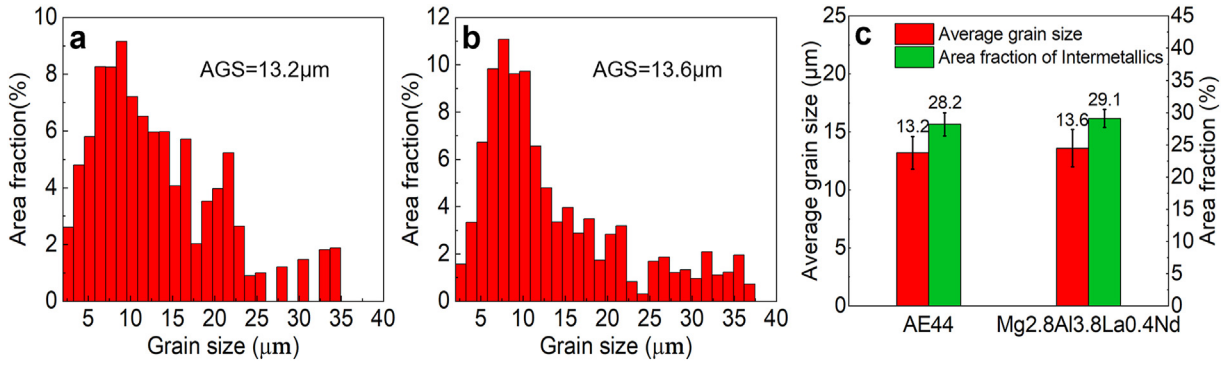

Fig. 11 – The AGS distribution and area fraction of intermetallic phases in die-cast Mg2.8Al3.8La0.4Nd and AE44 alloys at as-cast conditions. Grain size distribution of (a) AE44 and (b) Mg2.8Al3.8La0.4Nd alloys; (c) AGS and area fraction of intermetallic phases in die-cast Mg2.8Al3.8La0.4Nd and AE44 alloys.

where k_i is a constant that depends on the alloying element and temperature, C_i is the solute amount, and n is a constant equal to 1/2, 1, 2/3 [41,42]. According to Fig. 10, the RE, Mn and Zn content was similar in Mg2.8Al3.8La0.4Nd alloy and AE44 alloy. Therefore, the difference in σ_{ss} was mainly due to the Al solute amount. K_{Al} (=118 MPa (at.)$^{-1/2}$ and 196 MPa (at.)$^{-2/3}$) was the strengthening rate of solid solution based on binary alloys with n of 1/2 and 2/3, respectively [43,44]. Thus, the σ_{ss} of the Al dissolved in the matrix to Mg2.8Al3.8La0.4Nd alloy was 7.5 MPa and 4.9 MPa, respectively. The lower solid solution Al content in Mg2.8Al3.8La0.4Nd alloy resulted in smaller $\Delta\sigma_{ss}$ than in AE44 alloy, approximately −2.3 MPa. In contrast, the need for the high TC alloy development strategy made the strengthening effect produced by Al solid solution in Mg2.8Al3.8La0.4Nd alloy have less impact on the YS.

The Hall-Petch equation [30,45] can be used to express the $\Delta\sigma_{gr}$:

$$\Delta\sigma_{gr} = Kd^{-\frac{1}{2}} \quad (3)$$

K is the constant for Mg (280–320 MPa/μm$^{1/2}$), and d is the AGS [46,47]. Calculated from Fig. 11b, the effect of σ_{gr} on the YS of Mg2.8Al3.8La0.4Nd was approximately 101 MPa. From Fig. 11c, the AGS of Mg2.8Al3.8La0.4Nd alloy was higher than AE44 alloy. Al-RE phases, such as Al_2RE, have been reported to act as heterogeneous nucleation sites to refine grains [31]. However, there is no evidence that the $Al_{2.12}RE_{0.88}$ phase in Mg2.8Al3.8La0.4Nd alloys can refine grains as a heterogeneous nucleation site as the Al_2RE phase in the AE44 alloy. In addition, the formation of the Al-RE phase at grain boundaries was considered to prevent grain growth [31]. However, due to the generally small grain size in HPDC Mg alloys, the difference in grain size between the Mg2.8Al3.8La0.4Nd alloy and the AE44 alloy is insignificant. Thus, it was apparent that the σ_{gr} for Mg2.8Al3.8La0.4Nd alloy was lower than AE44 alloy, but the difference was minor, approximately −1.3 MPa.

Considering that σ_{ss} and σ_{gr} have a lower effect on Mg2.8Al3.8La0.4Nd alloy than on AE44 alloy, the increase in YS was mainly determined by the σ_{sp}. Integrating the results of σ_{ss} and σ_{gr}, the effect of σ_{sp} on Mg2.8Al3.8La0.4Nd alloy was approximately 28.6 MPa. According to Table 3, the experimental difference in YS between the two alloys was approximately 8 MPa. Integrated $\Delta\sigma_{ss}$ and $\Delta\sigma_{gr}$, the $\Delta\sigma_{sp}$ was considered to have a higher contribution to Mg2.8Al3.8La0.4Nd alloy than AE44 alloy, with a value of approximately 11.6 MPa. As shown in the analysis of intermetallic compounds in Section 3 and Fig. 11c, the most significant difference was that Mg2.8Al3.8La0.4Nd alloy had a higher fraction of the formed $(Al,Mg)_3RE$ phase than the dominant $Al_{11}RE_3$ phase in AE44 alloy. Therefore, it was evident that the increase in YS of Mg2.8Al3.8La0.4Nd alloy compared to commercial AE44 alloy was mainly due to the contribution of σ_{sp}. The decrease in room temperature ductility was expected to be related to the different deformation mechanisms of $(Al,Mg)_3RE$ and $Al_{11}RE_3$, hopefully providing cutting-edge in-situ deformation facilities for research shortly. Furthermore, lower Al solute in matrix reduced the precipitation of the low melting point $Mg_{17}Al_{12}$ phase, improving YS at HT. Also, the high content of the major $(Al,Mg)_3RE$ phase formation in GBs should contribute significantly to the enhancement of YS at HT. In addition, Fig. 3h shows that the Mg2.8Al3.8La0.4Nd alloy has excellent plasticity at HT. In general, α-Mg was more deformable at HT as more slip systems were activated, resulting in increased HT plasticity. In addition, the major intermetallic $(Al,Mg)_3RE$, $Al_{11}RE_3$, and $Al_{10}RE_2Mn_7$ phases formed in the Mg2.8Al3.8La0.4Nd alloy were all thermally stable phases. The $(Al,Mg)_3RE$ phase was reported to remain at 500 °C for 100 h without significant morphological changes [32], $Al_{11}RE_3$ had no visible decomposition at 450 °C [48], and the $Al_{10}RE_2Mn_7$ phase had a melting point of about 1150 °C [49]. Thus, the major intermetallic phases of the Mg2.8Al3.8La0.4Nd alloy can remain stable at up to 300 °C, thus pinning grain boundaries and impeding grain sliding. Therefore, the Mg2.8Al3.8La0.4Nd alloy obtained excellent mechanical properties at HT mainly due to the thermal stability of the major intermetallic phases.

5. Conclusions

A novel high TC and cost-effective die-cast Mg2.8Al3.8La0.4Nd alloy was successfully developed with the enhancement of YS at RT and HT, compared with AE44 alloy, and the major conclusions are as follows:

(1) Mg2.8Al3.8La0.4Nd alloy can provide the TC of 104.0 W/(m·K) at RT and 125.9 W/(m·K) at 300 °C, which are improved by 13.7% and 13.2%, respectively, compared with AE44 alloy. Importantly, the raw material cost of Mg2.8Al3.8La0.4Nd alloy is only 1.3% higher than AE44 alloy.
(2) Mg2.8Al3.8La0.4Nd alloy can deliver an excellent YS, UTS and elongation of 137.1 MPa, 240.2 MPa and 8.8% at RT. Compared with AE44 alloy, the YS of Mg2.8Al3.8-La0.4Nd alloy was enhanced by 6.3% at RT and 9.8% at 300 °C.
(3) Four intermetallic phases were identified in Mg2.8Al3.8La0.4Nd alloy, i.e., the lamellar $(Al,Mg)_3RE$ and $Al_{11}RE_3$ phases, the needle-like $Al_{2.12}RE_{0.88}$ phase and the blocky $Al_{10}RE_2Mn_7$ phase. Different from AE44 alloy, $(Al,Mg)_3RE$ formed and replaced $Al_{11}RE_3$ as the major intermetallic phase in Mg2.8Al3.8La0.4Nd alloy.
(4) The improvement in TC was mainly due to the decrease of Al solution in the matrix via optimizing Al and RE addition. The Al solute amount in the matrix of the Mg2.8Al3.8La0.4Nd alloy was decreased by 42% compared with AE44 alloy. The substitution formation of the major $(Al,Mg)_3RE$ intermetallic phase at GBs enhanced YS at RT and HT.

Credit author statement

L. Feng: experimental conduction, data analysis and manuscript preparation. **X. Dong:** Full-time supervision, conception, experimental design and conduction, results analysis, manuscript drafting and revision, manuscript proof. **M. Xia, X. Zhu & H. Yang:** Experimental assistance, result analysis and discussion. **G. Ji:** TEM characterisation. **B. Wang:** Result discussion, manuscript revision. **E. Nyberg:** Result discussion, proofreading. **S. Ji:** fund acquisition and manuscript proof.

Declaration of competing interest

The authors declare that they have no known competing financial interests or personal relationships that could have appeared to influence the work reported in this paper.

Acknowledgements

This work has been supported by the Innovate UK project (Project reference: 10004694) and Husqvarna Group. Mr Jon Gadd from BCAST and Brunel University London supported the high pressure die casting experiments.

Appendix A. Supplementary data

Supplementary data to this article can be found online at https://doi.org/10.1016/j.jmrt.2022.12.125.

REFERENCES

[1] Li S, Yang X, Hou J, Du W. A review on thermal conductivity of magnesium and its alloys. J Magnes Alloys 2020;8:78–90. https://doi.org/10.1016/j.jma.2019.08.002.
[2] Pollock TM. Materials science. Weight loss with magnesium alloys. Science 2010;328:986–7. https://doi.org/10.1126/science.1182848.
[3] Luo AA. Magnesium casting technology for structural applications. J Magnes Alloys 2013;1:2–22. https://doi.org/10.1016/j.jma.2013.02.002.
[4] Dong X, Feng L, Wang S, Ji G, Addad A, Yang H, et al. On the exceptional creep resistance in a die-cast Gd-containing Mg alloy with Al addition. Acta Mater 2022;232:117957. https://doi.org/10.1016/j.actamat.2022.117957.
[5] Dong X, Feng L, Wang S, Nyberg EA, Ji S. A new die-cast magnesium alloy for applications at higher elevated temperatures of 200–300 °C. J Magnes Alloys 2021;9:90–101. https://doi.org/10.1016/j.jma.2020.09.012.
[6] Pekguleryuz M. Alloying behavior of magnesium and alloy design. In: Pekguleryuz MO, Kainer K, Kaya A, editors. Fundam. Magnes. Alloy metall. Cambridge: Woodhead Publishing; 2013. p. 152–96.
[7] Dong X, Feng L, Wang S, Wang F, Ghasemi R, Ji G, et al. A quantitative strategy for achieving the high thermal conductivity of die-cast Mg-Al-based alloys. Materialia 2022;22:101426. https://doi.org/10.1016/j.mtla.2022.101426.
[8] Liu G, Karim M, Wang S, Eskin D, McKay B. Processing of SiC nano-reinforced AlSi9Cu3 composites by stir mixing, ultrasonication and high pressure die casting. J Mater Res Technol 2022;18:2384–98. https://doi.org/10.1016/j.jmrt.2022.03.132.
[9] Dong X, He L, Huang X, Li P. Effect of electromagnetic transport process on the improvement of hydrogen porosity defect in A380 aluminum alloy. Int J Hydrogen Energy 2015;40:9287–97. https://doi.org/10.1016/j.ijhydene.2015.05.160.
[10] Pan H, Pan F, Yang R, Peng J, Zhao C, She J, et al. Thermal and electrical conductivity of binary magnesium alloys. J Mater Sci 2014;49:3107–24. https://doi.org/10.1007/s10853-013-8012-3.
[11] Zhong L, Peng J, Sun S, Wang Y, Lu Y, Pan F. Microstructure and thermal conductivity of as-cast and as-solutionized Mg–rare earth binary alloys. J Mater Sci Technol 2017;33:1240–8. https://doi.org/10.1016/j.jmst.2016.08.026.
[12] Su C, Li D, Luo AA, Ying T, Zeng X. Effect of solute atoms and second phases on the thermal conductivity of Mg-RE alloys: a quantitative study. J Alloys Compd 2018;747:431–7. https://doi.org/10.1016/j.jallcom.2018.03.070.
[13] Wang C, Cui Z, Liu H, Chen Y, Ding W, Xiao S. Electrical and thermal conductivity in Mg-5Sn Alloy at different aging status. Mater Des 2015;84:48–52. https://doi.org/10.1016/j.matdes.2015.06.110.
[14] Dong XX, He LJ, Huang XS, Li PJ. Coupling analysis of the electromagnetic transport of liquid aluminum alloy during casting. J Mater Process Technol 2015;222:197–205. https://doi.org/10.1016/j.jmatprotec.2015.02.033.
[15] Zhong L, Wang Y, Gong M, Zheng X, Peng J. Effects of precipitates and its interface on thermal conductivity of Mg-12Gd alloy during aging treatment. Mater Char 2018;138:284–8. https://doi.org/10.1016/j.matchar.2018.02.019.
[16] Li ZH, Sasaki TT, Shiroyama T, Miura A, Uchida K, Hono K. Simultaneous achievement of high thermal conductivity, high strength and formability in Mg-Zn-Ca-Zr sheet alloy. Mater Res Lett 2020;8:335–40. https://doi.org/10.1080/21663831.2020.1759718.
[17] Zhong L, Peng J, Sun Y, Wang Y, Lu Y, Pan F. Microstructure and thermal conductivity of as-cast and as-extruded binary

Mg-Mn alloys. Mater Sci Technol 2017;33:92–7. https://doi.org/10.1080/02670836.2016.1161130.
[18] Luo AA. Recent magnesium alloy development for elevated temperature applications. Int Mater Rev 2004;49:13–30. https://doi.org/10.1179/095066004225010497.
[19] Prasad SVS, Prasad SB, Verma K, Mishra RK, Kumar V, Singh S. The role and significance of Magnesium in modern day research-A review. J Magnes Alloys 2021;10:1–61. https://doi.org/10.1016/j.jma.2021.05.012.
[20] Yuan G, You G, Bai S, Guo W. Effects of heat treatment on the thermal properties of AZ91D magnesium alloys in different casting processes. J Alloys Compd 2018;766:410–6. https://doi.org/10.1016/j.jallcom.2018.06.370.
[21] Mordike BL, Lukáč P. Physical metallurgy. In: Friedrich HE, Mordike BL, editors. Magnes. Technol. Metall. Des. Data appl. Berlin, Heidelberg: Springer; 2006. p. 63–107. https://doi.org/10.1007/3-540-30812-1_3.
[22] Meridian. Lightweight alloys 2022. https://www.meridian-mag.com/magnesium-die-casting/lightweight-alloys/ (accessed November 23, 2022).
[23] Dong X, Yang H, Zhu X, Ji S. High strength and ductility aluminium alloy processed by high pressure die casting. J Alloys Compd 2019;773:86–96. https://doi.org/10.1016/j.jallcom.2018.09.260.
[24] Feng L, Dong X, Cai Q, Wang B, Ji S. Effect of Nd on the microstructure and mechanical properties of Mg-La-Ce alloys at ambient and elevated temperatures. J Mater Eng Perform 2022. https://doi.org/10.1007/s11665-022-06853-x.
[25] He J, Chen J, Yan H, Xia W, Su B, Pan P, et al. Effect of Zn/Ga ratio on damping and thermal behaviors of fine-grained Mg-Zn-Ga sheets. J Mater Eng Perform 2022;31:5201–11. https://doi.org/10.1007/s11665-022-06605-x.
[26] Okamoto H. La-Mg (Lanthanum-Magnesium). J Phase Equilibria Diffus 2012;34:161–2. https://doi.org/10.1007/s11669-012-0166-1.
[27] Almgren M, Dong XX, Ji SX. A magnesium alloy and a high performance magnesium cylinder made from the magnesium alloy. Swedish Patent 2022:SE544427C2.
[28] Moreno IP, Nandy TK, Jones JW, Allison JE, Pollock TM. Microstructural characterization of a die-cast magnesium-rare earth alloy. Scripta Mater 2001;45:1423–9. https://doi.org/10.1016/s1359-6462(01)01179-4.
[29] Zhu SM, Gibson MA, Easton MA, Nie JF. The relationship between microstructure and creep resistance in die-cast magnesium–rare earth alloys. Scripta Mater 2010;63:698–703. https://doi.org/10.1016/j.scriptamat.2010.02.005.
[30] Feng L, Dong X, Cai Q, Wang B, Ji S. Effect of Gd on the microstructure and mechanical properties of high-pressure die-cast Mg-La-Ce alloys at ambient and elevated temperatures. J Alloys Compd 2022:923. https://doi.org/10.1016/j.jallcom.2022.166364.
[31] Zhu S, Wong C, Styles MJ, Abbott TB, Nie J-F, Easton MA. Revisiting the intermetallic phases in high-pressure die-cast Mg-4Al-4Ce and Mg-4Al-4La alloys. Mater Char 2019;156. https://doi.org/10.1016/j.matchar.2019.109839.
[32] Wong C, Styles MJ, Zhu S, Qiu D, McDonald SD, Zhu Y, et al. (Al,Mg)3La: a new phase in the Mg-Al-La system. Acta Crystallogr B Struct Sci Cryst Eng Mater 2018;74:370–5. https://doi.org/10.1107/S205252061800834X.
[33] Zhang J, Liu S, Leng Z, Liu X, Niu Z, Zhang M, et al. Structure stability and mechanical properties of high-pressure die-cast Mg-Al-La-Y-based alloy. Mater Sci Eng, A 2012;531:70–5. https://doi.org/10.1016/j.msea.2011.10.025.
[34] Zhu SM, Abbott TB, Gibson MA, Nie JF, Easton MA. Age hardening in die-cast Mg-Al-RE alloys due to minor Mn additions. Mater Sci Eng, A 2016;656:34–8. https://doi.org/10.1016/j.msea.2016.01.012.
[35] Pettersen G, Westengen H, Høier R, Lohne O. Microstructure of a pressure die cast magnesium—4wt.% aluminium alloy modified with rare earth additions. Mater Sci Eng, A 1996;207:115–20. https://doi.org/10.1016/0921-5093(95)10035-0.
[36] Su C, Li D, Ying T, Zhou L, Li L, Zeng X. Effect of Nd content and heat treatment on the thermal conductivity of Mg Nd alloys. J Alloys Compd 2016;685:114–21. https://doi.org/10.1016/j.jallcom.2016.05.261.
[37] Dong H, Wen B, Melnik R. Relative importance of grain boundaries and size effects in thermal conductivity of nanocrystalline materials. Sci Rep 2014;4:7037. https://doi.org/10.1038/srep07037.
[38] Dong X, Zhang Y, Amirkhanlou S, Ji S. High performance gravity cast Al9Si0.45Mg0.4Cu alloy inoculated with AlB 2 and TiB 2. J Mater Process Technol 2018;252:604–11. https://doi.org/10.1016/j.jmatprotec.2017.10.028.
[39] Dong X, Youssef H, Zhu X, Zhang Y, Wang S, Ji S. High as-cast strength die-cast AlSi9Cu2Mg alloy prepared by nanoparticle strengthening with industrially acceptable ductility. J Alloys Compd 2021;852:156873. https://doi.org/10.1016/j.jallcom.2020.156873.
[40] Gao L, Chen RS, Han EH. Microstructure and strengthening mechanisms of a cast Mg-1.48Gd-1.13Y-0.16Zr (at.%) alloy. J Mater Sci 2009;44:4443–54. https://doi.org/10.1007/s10853-009-3672-8.
[41] Gypen LA, Deruyttere A. Multi-component solid solution hardening. J Mater Sci 1977;12:1034–8. https://doi.org/10.1007/BF00540988.
[42] Gao L, Chen RS, Han EH. Effects of rare-earth elements Gd and Y on the solid solution strengthening of Mg alloys. J Alloys Compd 2009;481:379–84. https://doi.org/10.1016/j.jallcom.2009.02.131.
[43] Cáceres CH, Rovera DM. Solid solution strengthening in concentrated Mg-Al alloys. J Light Met 2001;1:151–6. https://doi.org/10.1016/S1471-5317(01)00008-6.
[44] Xu Y, Gensch F, Ren Z, Kainer KU, Hort N. Effects of Gd solutes on hardness and yield strength of Mg alloys. Prog Nat Sci Mater Int 2018;28:724–30. https://doi.org/10.1016/j.pnsc.2018.10.002.
[45] Hutchinson CR, Nie JF, Gorsse S. Modeling the precipitation processes and strengthening mechanisms in a Mg-Al-(Zn) AZ91 alloy. Metall Mater Trans A 2005;36:2093–105. https://doi.org/10.1007/s11661-005-0330-x.
[46] Hou C, Qi F, Ye Z, Zhao N, Zhang D, Ouyang X. Effects of Mn addition on the microstructure and mechanical properties of Mg-Zn-Sn alloys. Mater Sci Eng, A 2020;774. https://doi.org/10.1016/j.msea.2020.138933.
[47] Cheng WL, Tian QW, Yu H, Zhang H, You BS. Strengthening mechanisms of indirect-extruded Mg-Sn based alloys at room temperature. J Magnes Alloys 2014;2:299–304. https://doi.org/10.1016/j.jma.2014.11.003.
[48] Zhu S, Abbott TB, Nie J-F, Ang HQ, Qiu D, Nogita K, et al. Re-evaluation of the mechanical properties and creep resistance of commercial magnesium die-casting alloy AE44. J Magnes Alloys 2021;9:1537–45. https://doi.org/10.1016/j.jma.2021.04.016.
[49] Yang Q, Lv S-H, Meng F-Z, Guan K, Li B-S, Zhang X-H, et al. Detailed structures and formation mechanisms of well-known Al10RE2Mn7 phase in die-cast Mg-4Al-4RE-0.3Mn alloy. Acta Metall Sin Engl Lett 2019;32:178–86. https://doi.org/10.1007/s40195-018-0819-0.